Limnol. Oceanogr., 49(6), 2004, 2058–2072

Quantification of macrobenthic effects on diagenesis using a multicomponent inverse model in salt marsh sediments

Yoko Furukawa[1]
Naval Research Laboratory, Seafloor Sciences Branch, Stennis Space Center, Mississippi 39529

April C. Smith and Joel E. Kostka
Department of Oceanography, Florida State University, Tallahassee, Florida 32306

Janet Watkins
Naval Research Laboratory, Seafloor Sciences Branch, Stennis Space Center, Mississippi 39529

Clark R. Alexander
Skidaway Institute of Oceanography, Savannah, Georgia 31411

Abstract

Using a multicomponent inverse model, we quantified the rates of organic matter (OM) remineralization and the relative importance of major terminal electron acceptors [Fe(III)-(oxy)hydroxides and SO_4^{2-}] in salt marsh sediments with varying degrees of bioturbation and vegetation at Skidaway Island, Georgia. The model determined the rates of OM diagenesis by seeking simultaneous agreement between measured and model-calculated depth-concentration profiles of multiple major redox species while using the biological transport parameters determined from direct field observations. The OM degradation rates are found to be greater and penetrate deeper in sediments with vegetation or bioturbation than in sediments with limited macrobenthic components, in which organic matter degradation is restricted to the immediate vicinity of water-sediment interface. The results also confirmed previous observations that Fe(III)-(oxy)hydroxides are much more important than sulfate as terminal electron acceptors in the heavily bioturbated station and provided the numerical values to the depth-dependent relative importance. Solid-phase Fe is recycled as a terminal electron acceptor $\geq$30 times in the bioturbated station, because biological mixing repeatedly moves reduced Fe(II) back into the aerobic environment, where it is reoxidized to form Fe(III)-(oxy)hydroxides and is reused as a terminal electron acceptor. Vegetation appears to have little influence on net solute transport, but it stimulates microbial activities and significantly enhances the remineralization of OM at depths.

The salt marsh is a complex geochemical system with highly coupled, simultaneous processes such as primary production, microbial degradation of organic matter (OM), and macrobenthos feeding. Along the east coast of the United States, salt marsh primary production is dominated by a species of smooth cordgrass, *Spartina alterniflora*, whose root systems are the conduits for chemical exchange between sediments and overlying water or air, as well as the primary source of OM to sedimentary microbial communities (Childers et al. 1993). Salt marsh sediments are often heavily bioturbated by fiddler crabs, *Uca* spp. (Teal 1958). These macrobenthos are directly involved in chemical mass transfer by producing and metabolizing OM and mobilizing chemicals (Kristensen et al. 1991; Nithart et al. 1999), while indirectly affecting the course of diagenesis by modifying microbial habitats (Goni-Urriza et al. 1999; Marinelli et al. 2002). The complete characterization of salt marsh system benefits from a comprehensive approach in which all critical processes are considered concurrently in a coupled manner. Computational reactive transport modeling has become an effective tool for the comprehensive descriptions of aquatic sedimentary systems undergoing early diagenesis.

A unique utility of properly constrained modeling is the ability to quantify properties and processes that cannot be directly measured, such as the in situ rates of OM degradation and terminal electron acceptor (TEA) reduction. In diagenetic modeling, forward modeling proceeds by interactively comparing model-calculated concentration profiles of geochemical species to measured profiles, whereas inverse modeling uses measured profiles as a direct forcing to determine hard-to-measure properties such as reaction rates and transport coefficients. Using directly measured or estimated forcing variables (e.g., sediment accumulation rates, biological reworking depth, and overlying water chemistry), previous forward modeling studies have hind-casted the rates of Fe and Mn cycling in shelf sediments (Van Cappellen and Wang 1996), rates and mechanisms of denitrification at the global scale (Middelburg et al. 1996), and redox oscillation along infauna burrows (Furukawa 2001). The inverse approach has been used to determine consumption rates of major redox species (Berg et al. 1998), and bioirrigation coefficients (Meile et al. 2001).

[1] Corresponding author (yfurukawa@nrlssc.navy.mil).

Acknowledgments

Dava Dalton, Chad Vaughan, Sherry Dollhopf, Mike Dollhopf, Haley Skelton, Lanie Petrie, Harold Adams, and Steve Smith provided field and laboratory assistance.

This study was funded by ONR322MG and NRL/ONR Core funds.

This is NRL contribution NRL/JA/7430-03-5.

Table 1. Geochemical species and reactions considered in this study

Porewater species	
O_2	Oxygen
NO_3^-	Nitrate
NH_4^+	Ammonium
SO_4^{2-}	Sulfate
TS	Aqueous sulfide species ($=H_2S + HS^-$)
Fe^{2+}	Ferrous ion
ΣCO_2	$H_2CO_3 + HCO_3^- + CO_3^{2-}$
Particulate species	
OM	Organic matter with the model formula of $(CH_2O)(NH_4^+)_{y/x}$, where x : y is the C : N ratio
$Fe(OH)_3$	Poorly crystalline Fe(III)-(oxy)hydroxides expressed as $Fe(OH)_3$
FeS	Precipitated ferrous sulfides
NH_4(ads)	Surface-adsorbed ammonium

Primary redox reactions:	Rates:
$OM + O_2 \rightarrow \Sigma CO_2 + \frac{y}{x}NH_4^+ + H_2O$	R_1 (mol dm^{-3}-solids s^{-1})
$OM + 0.8NO_3^- + 0.8H^+ \rightarrow \Sigma CO_2 + \frac{y}{x}NH_4^+ + 0.4N_2 + 1.4H_2O$	R_2 (mol dm^{-3}-solids s^{-1})
$OM + 4Fe(OH)_3 + 8H^+ \rightarrow \Sigma CO_2 + \frac{y}{x}NH_4^+ + 4Fe^{2+} + 11H_2O$	R_3 (mol dm^{-3}-solids s^{-1})
$OM + 0.5SO_4^{2-} + H^+ \rightarrow \Sigma CO_2 + \frac{y}{x}NH_4^+ + 11H_2O + 0.5H_2S$	R_4 (mol dm^{-3}-solids s^{-1})
Secondary reactions:	**Rates:**
$Fe^{2+} + \frac{1}{4}O_2 + \frac{5}{2}H_2O \rightarrow Fe(OH)_3 + 2H^+$	R_5 (mol L^{-1}-porewater s^{-1})
$NH_4^+ + 2O_2 \rightarrow NO_3^- + H_2O + 2H^+$	R_6 (mol L^{-1}-porewater s^{-1})
$H_2S + 2O_2 \rightarrow SO_4^{2-} + 2H^+$	R_7 (mol L^{-1}-porewater s^{-1})
$\frac{1}{2}H_2S + Fe(OH)_3 + 2H^+ \rightarrow \frac{1}{2}S^0 + Fe^{2+} + 3H_2O$	R_8 (mol dm^{-3}-solids s^{-1})
$FeS + 2O_2 \rightarrow Fe^{2+} + SO_4^{2-}$	R_9 (mol dm^{-3}-solids s^{-1})
$Fe^{2+} + H_2S \rightarrow FeS + 2H^+$	R_{10} (mol L^{-1}-porewater s^{-1})
Equilibrium reactions:	**Equilibrium constant:**
$NH_4^+ \leftrightarrow NH_4^+$(ads)	k_N

Recent studies in salt marshes of the U.S. Atlantic coast have documented the significant recycling of iron and sulfur, and complex spatial overlapping of the TEA sequences (Luther et al. 1986; Kostka et al. 2002*a*; Gribsholt et al. 2003; Koretsky et al. 2003). This recycling has been attributed to the repeated reoxidation of reduced iron and sulfur caused by bioturbation, bioirrigation, and phytoirrigation. Because of the inherent complexity of salt marsh systems, it is difficult to quantify OM remineralization pathways by experimental methods alone. A modeling approach in which all critical reactions and transport processes are simultaneously considered would allow comprehensive and quantitative descriptions of the complex systems.

The objective of the present study was to quantify the rates and pathways of OM remineralization through multicomponent inverse modeling constrained by extensive field data. The realistic model descriptions of biological transport processes were emphasized, to assess their effect on diagenetic chemical mass transfer. The inverse modeling allowed the extraction of hard-to-measure parameters using directly measured variables. We simultaneously applied inverse modeling to concentration profiles of multiple species, to minimize the uncertainties in model results generated by the independent uncertainties in rate description of each individual species.

Materials and methods

Reactions and rate expressions—The geochemical species and reactions considered in the study are defined in Table 1. OM degradation pathways in the upper ~0.5 m of salt marsh sediments have been considered to be dominated by microbial SO_4^{2-} respiration (Howarth and Giblin 1983; King 1988), whereas recent studies have shown evidence for the importance of Fe(III)-(oxy)hydroxide respiration (Lowe et al. 2000; Kostka et al. 2002*a*). Therefore, we investigated these, in addition to the respiration of O_2 and NO_3^-, as the primary redox reactions. The reaction expressions are based on those found in previous work (Froelich et al. 1979; Van Cappellen and Wang 1996), which have been tested in the context of multicomponent reactive transport models (Boudreau 1996*b*; Archer et al. 2002). The reactions have since been updated to express the inorganic nitrogen product of

aerobic OM degradation to be NH_4^+ rather than NO_3^- (Herbert 1999; Berg et al. 2003).

On the basis of the reactions in Table 1, the rates of primary and secondary reactions, as well as the net production rates of geochemical species, can be expressed (Table 2). The OM degradation rates are considered to follow *Monod* kinetics (Boudreau 1996*a*), whereas the secondary reactions are presumed to follow the simple bimolecular rate laws that are widely used in multicomponent reactive transport models (Van Cappellen and Wang 1996; Berg et al. 2003).

Mass conservation equations—The multicomponent inverse model used in the study is based on the one-dimensional mass conservation equation. For solute species, it can be written as

$$\frac{\partial C}{\partial t} = \frac{1}{\varphi}\frac{\partial}{\partial x}\left[\varphi(D_S + D_B)\frac{\partial C}{\partial x} - \varphi w C\right] + \alpha(C_0 - C) + \Sigma R \tag{1}$$

or under the no-compaction (i.e., constant porosity) assumption,

$$\frac{\partial C}{\partial t} = \frac{\partial}{\partial x}\left[(D_S + D_B)\frac{\partial C}{\partial x}\right] - w\frac{\partial C}{\partial x} + \alpha(C_0 - C) + \Sigma R \quad (1')$$

(Berner 1980; Boudreau 1996*a*), in which the time (t, s)–dependent concentration of a dissolved species (C, mol L^{-1} pore water) along the vertical axis (x, m) is determined by its diffusive transport, accumulation due to sedimentation, transport by irrigation, and net rate of production and consumption reactions (ΣR, mol L^{-1} s^{-1}). D_S (m^2 s^{-1}) is the tortuosity-corrected molecular diffusion coefficient, D_B (m^2 s^{-1}) is the biodiffusion coefficient, φ is the porosity, α (m^{-1}) is the bioirrigation coefficient, w is the sediment accumulation rate (m s^{-1}), and C_0 (mol L^{-1}) is the concentration at water-sediment interface (WSI). Similarly, the mass conservation equation for solid species can be written as

$$\frac{\partial C_s}{\partial t} = \frac{\partial}{\partial x}\left(D_B\frac{\partial C_s}{\partial x}\right) - w\frac{\partial C_s}{\partial x} + \Sigma R_s \tag{2}$$

where C_s is the concentration of the solid species (mol dm^{-3} of solids) and ΣR_s is the net rate of production (mol dm^{-3} solids s^{-1}). Irrigation and molecular diffusion are not considered for solids.

The partial discretization of Eq. 1′ for the ith node on an even grid yields an ordinary differential equation (ODE):

$$\begin{aligned}\frac{dC_i}{dt} = {} & D_i\frac{C_{i+1} - 2C_i + C_{i-1}}{\Delta x^2} \\ & + \left(\frac{D_{i+1} - D_{i-1}}{2\Delta x} - w\right) \\ & \times \left[\frac{(1 - \sigma_i)C_{i+1} + 2\sigma_i C_i - (1 + \sigma_i)C_{i-1}}{2\Delta x}\right] \\ & + \alpha_i(C_0 - C_i) + \Sigma R_i\end{aligned} \tag{3}$$

where

$$\sigma_i = \coth\left(\frac{w\Delta x}{2D_i}\right) - \frac{2D_i}{w\Delta x} \tag{4}$$

(Boudreau 1996*a*). C_i (mol L^{-1}) and D_i (m^2 s^{-1}) denote the concentration and net diffusion coefficient ($D_s + D_B$) at the ith node, and Δx is the distance between adjacent nodes. A similar ODE can be written for solid species by partially discretizing Eq. 2.

By assuming that the geochemical profiles are at steady state, the left-hand side of Eq. 3 is set at $dC_i/dt = 0$, and the right-hand side can be reorganized as

$$aa_i C_{i-1} + bb_i C_i + cc_i C_{i+1} + dd_i = 0 \tag{5}$$

where

$$aa_i = \frac{D_i}{\Delta x^2} - \left(\frac{1 + \sigma_i}{2\Delta x}\right)\left(\frac{D_{i+1} - D_{i-1}}{2\Delta x} - w\right) \tag{6a}$$

$$bb_i = -\frac{2D_i}{\Delta x^2} + \left(\frac{\sigma_i}{\Delta x}\right)\left(\frac{D_{i+1} - D_{i-1}}{2\Delta x} - w\right) - \alpha_i \tag{6b}$$

$$cc_i = \frac{D_i}{\Delta x^2} + \left(\frac{1 - \sigma_i}{2\Delta x}\right)\left(\frac{D_{i+1} - D_{i-1}}{2\Delta x} - w\right) \tag{6c}$$

$$dd_i = \alpha_i C_0 + \Sigma R_i \tag{6d}$$

If we use the known concentrations at WSI (i.e., $x = 0$, first node), C_0, and at the bottom of modeled sediment column (i.e., $x = L_b$, nth node), C_b, as the boundary conditions, then

$$C_{i=1} = C_0; \text{ and } C_{i=n} = C_b \tag{7}$$

As a consequence, the series of equations can be written as

$$\begin{pmatrix} bb_1 & cc_1 & & & & & \\ aa_2 & bb_2 & cc_2 & & & & \\ & & \ddots & & & & \\ & aa_{i-1} & bb_{i-1} & cc_{i-1} & & & \\ & & aa_i & bb_i & cc_i & & \\ & & & aa_{i+1} & bb_{i+1} & cc_{i+1} & \\ & & & & \ddots & & \\ & & & & aa_{n-1} & bb_{n-1} & cc_{n-1} \\ & & & & & aa_n & bb_n \end{pmatrix} \times \begin{pmatrix} C_1 \\ C_2 \\ \vdots \\ C_{i-1} \\ C_i \\ C_{i+1} \\ \vdots \\ C_{n-1} \\ C_n \end{pmatrix} + \begin{pmatrix} dd_1 \\ dd_2 \\ \vdots \\ dd_{i-1} \\ dd_i \\ dd_{i+1} \\ \vdots \\ dd_{n-1} \\ dd_n \end{pmatrix} = 0 \quad \text{or} \tag{8a}$$

$$ABC \times C + DD = 0 \tag{8b}$$

in which C and DD are vectors and ABC is a tridiagonal matrix.

Table 2. Rate expressions and net reaction rates considered in this study

Notation

Reaction rate expressions:

$$R_1 = kG\frac{[O_2]}{K_{O_2} + [O_2]}$$

$$R_2 = kG\frac{[NO_3^-]}{K_{NO_3} + [NO_3^-]}\frac{K'_{O_2}}{K'_{O_2} + [O_2]}$$

$$R_3 = kG\frac{[Fe(OH)_3]}{[Fe(OH)_3]_0}\frac{K'_{NO_3}}{K'_{NO_3} + [NO_3^-]}\frac{K'_{O_2}}{K'_{O_2} + [O_2]}$$

$$R_4 = kG\frac{[SO_4^{2-}]}{K_{SO_4} + [SO_4^{2-}]}\frac{1}{1 + \frac{K'_{Fe(OH)_3}[Fe(OH)_3]}{[Fe(OH)_3]_0}}\frac{K'_{NO_3}}{K'_{NO_3} + [NO_3^-]}\frac{K'_{O_2}}{K'_{O_2} + [O_2]}$$

$$R_5 = k_5[Fe^{2+}][O_2] \qquad R_6 = k_6[NH_4^+][O_2] \qquad R_7 = k_7[TS][O_2]$$

$$R_8 = k_8[TS][Fe(OH)_3] \qquad R_9 = k_9[FeS][O_2] \qquad R_{10} = k_{10}[Fe^{2+}][TS]$$

where kG is the rate of organic carbon remineralization (mol C dm^{-3}-solid s^{-1}), K_{O_2}, K_{NO_3}, and K_{SO_4} are the Monod saturation constants, and K'_{O_2}, K'_{NO_3}, and $K'_{Fe(OH)_3}$ are the Monod inhibition constants.

Equilibrium expression:

$$[NH_4^+(ads)] = \frac{\varphi}{\rho(1-\varphi)}k_N[NH_4^+] \quad \text{where } \rho \text{ is the sediment density.}$$

Net production rates:

$$\Sigma R_{O_2} = \frac{1-\varphi}{\varphi}R_1 - \frac{1}{4}R_5 - 2R_6 - 2O_7 - 2\frac{1-\varphi}{\varphi}R_9$$

$$\Sigma R_{NO_3^-} = -0.8R_2 + R_6$$

$$\Sigma R_{Fe(OH)_3} = -4R_3 + \frac{\varphi}{1-\varphi}R_5 - R_8$$

$$\Sigma R_{SO_4^{2-}} = -\frac{1-\varphi}{\varphi}\frac{1}{2}R_4 + R_7 + \frac{1-\varphi}{\varphi}R_9$$

$$\Sigma R_{Fe^{2+}} = 4\frac{1-\varphi}{\varphi}R_3 - R_5 + \frac{1-\varphi}{\varphi}R_8 + \frac{1-\varphi}{\varphi}R_9 - R_{10}$$

$$\Sigma R_{NH^{4+}} = \frac{1-\varphi}{\varphi}\frac{y}{x}(R_1 + R_2 + R_3 + R_4) - R_6$$

$$\Sigma R_{TS} = \frac{1}{2}\frac{1-\varphi}{\varphi}R_4 - R_7 - \frac{1}{2}\frac{1-\varphi}{\varphi}R_8 - R_{10}$$

$$\Sigma R_{FeS} = -R_9 + \frac{\varphi}{1-\varphi}R_{10}$$

$$\Sigma R_{\Sigma CO_2} = \frac{1-\varphi}{\varphi}(R_1 + R_2 + R_3 + R_4)$$

Inverse modeling strategy for rate determination—The objective of inverse modeling in the present study was to determine ΣR (and, thus, kG) as a function of depth (x). As shown in Table 2, ΣR values are the functions of kG, if the values of C, $k_5 \sim k_{10}$, k_N, and φ are known a priori. One important attribute of the study is the a priori derivation of D_B and α. Whereas most previous studies treated D_B and α as adjustable, we assigned them a range of a priori values based on the burrow and O_2 microprofile data, as described below. A simple matrix manipulation of (8–2) yields

$$C = -ABC^{-1} \times DD \tag{9}$$

which indicates that the concentration of the given species sp1 at the ith node can be expressed as a function of a priori parameters and net reaction rate, which is, in turn, a function of a priori parameters and kG,

$$C^{sp1}_{\text{calc},i} = f_1(D^{sp1}_{i-1}, D^{sp1}_i, D^{sp1}_{i+1}, \alpha^{sp1}_i, \Sigma R^{sp1}_i) \quad (10)$$

$$\Sigma R^{sp1}_i = f_2(kG, C^{sp1}_{\text{measured},i}, C^{sp2}_{\text{measured},i}, C^{sp3}_{\text{measured},i}, \ldots) \quad (11)$$

When Eqs. 10 and 11 are combined, *kG* is the only unknown. It should be noted that ΣR^{sp1}_i is a function not only of $C^{sp1}_{\text{measured},i}$ but also of the measured concentrations of other species.

In practice, the inverse determination of the *kG* profile progresses as follows. First, a randomly generated set of initial values are assigned to kG_1, kG_2, . . ., kG_n. It is assumed that *kG* value remains constant within each 0.01 m vertical section. Then, the *kG* values are used in Eqs. 9–11 to calculate the concentration profiles for NO_3^-, $Fe(OH)_3$, SO_4^-, and NH_4^+. Next, to pursue the simultaneous agreement between C_{calc} and C_{measured} for the multiple major redox species, the differences between C_{calc} and C_{measured} profiles are evaluated as

$$\Sigma F = \sum_{i=1}^{n} \frac{|C_{\text{calc},i} - C_{\text{measured},i}|^{NO_3^-}}{C^{NO_3^-}_{\max}} + \sum_{i=1}^{n} \frac{|C_{\text{calc},i} - C_{\text{measured},i}|^{Fe(OH)_3}}{C^{Fe(OH)_3}_{\max}} + \sum_{i=1}^{n} \frac{|C_{\text{calc},i} - C_{\text{measured},i}|^{SO_4^{2-}}}{C^{SO_4^{2-}}_{\max}} + \sum_{i=1}^{n} \frac{|C_{\text{calc},i} - C_{\text{measured},i}|^{NH_4^+}}{C^{NH_4^+}_{\max}} \quad (12)$$

where $C^{\text{species}}_{\max}$ denotes the highest measured concentration of the given species within the profile under consideration. Subsequently, the *kG* values are adjusted to find the optimized set of values until the value of ΣF is minimized according to the trust region methods for nonlinear minimization (Coleman and Li 1996), using a routine supplied in MATLAB Optimization Toolbox (The Mathworks, Inc.). To ensure that the optimization leads to the global minima rather than to local minima, the process is repeated up to 50 times, each with a new, randomly generated initial *kG* value.

Forward calculations of depth-concentration profiles—Once the depth profile of *kG* is determined, it is then used in the forward modeling to calculate the depth profiles of species listed in Table 1. In the forward modeling, Eq. 3 is written for each species using the same D_i, w, and α_i values used in the inverse modeling and solved for C_i by integrating for time using a stiff ODE solver in Matlab (ode23tb). ΣR_i is a function of *kG*, which is now a ''known'' parameter, and of C_i values of multiple species that are now treated as unknowns. Because the net rate of a given species is related to the concentrations of multiple species (Eq. 11), the integration of Eq. 3 for all species must occur simultaneously with the rate expressions being coupled for each time step (Boudreau 1996*b*).

Study area and methods

We used extensive field data obtained from muddy sediments of the Saltmarsh Ecosystem Research Facility (SERF) adjacent to the Skidaway Institute of Oceanography, Georgia, during August 2001. The sampling took place during low tide in the mid- to late-morning hours. The sediment temperatures were 27–28°C, and salinity of water from the drainage creek was 30. Data obtained from three stations are discussed here, which differed in the abundance of *Uca pugnax* as well as the density of *S. alterniflora* vegetation. The first station, designated BUC, is heavily bioturbated by *U. pugnax* and polychaetes but contains no vegetation. The second station, NUC, hosts neither *Spartina* nor *Uca* but is populated with a small number of polychaetes. The third station, NVC, hosts abundant *S. alterniflora* and a small number of polychaetes but no *Uca.* The station designation follows the convention used by the previous studies at SERF (Kostka et al. 2002*a*; Gribsholt et al. 2003).

Ecological measurements—The radius, opening density, and depth dependency of polychaete burrows were determined using X-radiographs, as described elsewhere (Furukawa et al. 2001). The corer used for X-radiography was 17 cm wide, 2.2 cm thick, and ~50 cm tall. Because the number of *Uca* burrows captured in the corers was too small for statistical considerations, depth dependency of *Uca* burrows was obtained from the literature (Basan and Frey 1977). The opening density and radii of *Uca* burrows were determined directly in the field, as described elsewhere (Gribsholt et al. 2003) using a 25 × 25 cm^2 quadrant.

Porewater and solid-phase geochemistry—The depth profiles of NO_3^-, SO_4^-, NH_4^+, total salinity (TS), Fe^{2+}, FeS, and $Fe(OH)_3$ were determined from 1- to 2-cm sections of triplicate cores for each station, as described elsewhere (Kostka et al. 2002*a*; Gribsholt et al. 2003). The O_2 microprofiles at the WSI were obtained with Clark-type microelectrodes from freshly sampled cores. The radial O_2 microprofiles at *Uca* burrow walls were obtained by inserting the microelectrode at a 45° angle. The microelectrodes were calibrated by oxygenated tap water whose O_2 concentration was known from Winkler titrations and by assuming that the constant current reading obtained by inserting the microelectrode tips deeply into the sediments away from burrow walls corresponds to $[O_2] = 0$ mol L^{-1}. It should be noted that the calibration was done with the low salinity tap water; thus, the data may overestimate the actual O_2 concentrations in pore water by several percent (Glud et al. 2000).

Radionuclide profiles—The depth profiles of ^{137}Cs were obtained from centimeter-thick sections of duplicate cores (Alexander et al. 1991; Sommerfield et al. 1999). Each sample of dried, ground sediment was counted for ~24 h on a planar ORTEC Lo-AX detector, to quantify ^{137}Cs activity at 661 KeV. Self-adsorption corrections were made using established techniques (Cutshall et al. 1983). Errors were estimated from the 1-SD confidence level of counting statistics to be ~10%.

Sulfate reduction rates (SSRs)—SRRs were determined on 10-cm triplicate cores (2 cm inner diameter) with $^{35}SO_4^{2-}$ (Fossing and Jørgensen 1989). Cores were stored at the in situ temperature for ≤2 h before injection. The $^{35}SO_4^{2-}$ was

Table 3. Model parameters.

Parameter	Values	Remarks
Concentration parameters		
$[NO_3]_0$	2.5×10^{-6}	Measured during 1987–1996 at Skidaway River (Verity 2002) (mol L^{-1})
$[NF_4^+]_0$	0	Estimated (mol L^{-1})
$[TS]_0$, $[Fe^{2+}]_0$	0	Estimated (mol L^{-1})
$[SO_4^{2-}]_0$	**0.029** (BUC); **0.023** (NUC); **0.023** (NVC)	Measured (this study) (mol L^{-1})
$[Fe(OH)_3]_0$	0.7	Estimated from $Fe(OH)_3$ and FeS profiles (mol dm^{-3})
Transport parameters		
φ	**0.860** (BUC); **0.821** (NUC); **0.859** (NVC)	Measured porosity (depth independent)
$D^0_{O_2}$ (m^2 s^{-1})	2.36×10^{-9}	Diffusion coefficients for infinite dilution is determined using the tables provided by Boudreau (1996*a*) with measured temperature (28°C) and salinity (30). The tortuosity correction follows the equations $D_S = D^0/\theta^2$ $\theta^2 = 1 - 2\ln(\phi^2)$ (Boudreau 1996*a*)
$D^0_{NO_3}$ (m^2 s^{-1})	2.00×10^{-9}	
$D^0_{NH_4}$ (m^2 s^{-1})	2.07×10^{-9}	
$D^0_{SO_4}$ (m^2 s^{-1})	1.11×10^{-9}	
$D^0_{H_2S}$ (m^2 s^{-1})	1.83×10^{-9}	
D^0_{HS} (m^2 s^{-1})	1.78×10^{-9}	
$D^0_{Fe(II)}$ (m^2 s^{-1})	7.36×10^{-10}	
$D^0_{H_2CO_3}$ (m^2 s^{-1})	1.87×10^{-9}	
$D^0_{HCO_3}$ (m^2 s^{-1})	1.25×10^{-9}	
$D^0_{CO_3}$ (m^2 s^{-1})	0.97×10^{-9}	
Reaction parameters		
k_5 (L mol^{-1} s^{-1})	5.9	(Zhang and Millero 1993)
k_6 (L mol^{-1} s^{-1})	0.63	(Berg et al. 2003)
k_7 (L mol^{-1} s^{-1})	0.039	(Millero et al. 1987)
k_8 (L mol^{-1} s^{-1})	7.0×10^{-4}	(Van Cappellen and Wang 1996; Boudreau et al. 1998)
k_9 (L mol^{-1} s^{-1})	0.7	(Van Cappellen and Wang 1996; Boudreau et al. 1998)
k_{10}	0.47	(Berg et al. 2003)
K_{O_2}, K'_{O_2}	8.0×10^{-6}	Monod constants (Boudreau et al. 1998)
K_{NO_3}, K'_{NO_3}	3.0×10^{-5}	Monod constants (Boudreau et al. 1998)
K_{SO_4}	0.001	Monod constants (Boudreau et al. 1998)
$K'_{Fe(OH)_3}$	2.70×10^{-1}	Monod constants (Boudreau et al. 1998)
k_N	1.4	NH_4^+ adsorption coefficient (Mackin and Aller 1984)

injected at 1-cm intervals, and cores were incubated at *in situ* temperature for 3 h. The cores were then sectioned into 1–2 cm intervals, fixed in 10 ml 20% ZnAc, and frozen. Total reduced sulfur (TRS; i.e., acid-volatile sulfides, FeS + TS plus chromium-reducible sulfur, $S^0 + FeS_2$) was extracted by a 45-min single-step distillation with cold HCl (2 mol L^{-1}) and boiling Cr^{2+} (0.5 mol L^{-1}) solutions. Color observation ensured the complete reduction by Cr. TRS in the distillate was determined spectrophotometrically, whereas $TR^{35}S$ activity was determined by a scintillation counter. Pore water was removed before distillations and was also analyzed for $^{35}SO_4^{2-}$. Total SO_4^{2-} was analyzed by ion chromatograph for use in calculating rates. SRRs were determined as the amount of $^{35}SO_4^{2-}$ reduced per hour, under the assumption that rates were constant during the 3-h incubation.

Parameter determination

Parameters required for the inverse and forward modeling are listed in Table 3. The values in Table 3 that are in boldface were determined through direct observations during the field study. The WSI is well exposed to air or oxygenated estuarine water; thus, the concentrations of reduced species at the WSI were estimated to be zero. The parameterization of Eqs. 9–11 for NO_3^-, $Fe(OH)_3$, SO_4^{2-}, and NH_4^+ required $C_{measured}$ profiles for O_2, NO_3^-, $Fe(OH)_3$, SO_4^{2-}, Fe^{2+}, TS, NH_4^+, and FeS (*see Table 2*). The $C_{measured}$ for O_2 was determined using the directly measured microprofiles plus burrow distribution statistics. $C_{measured}$ for other species was taken from the sample analysis and interpolated. The φ was measured in cores by weighing a known volume of sediment subsamples before and after drying. D_S, which was assumed to be depth independent, was determined from its empirical dependence on φ (Boudreau 1996*a*). D_B and α were determined using the burrow statistics, and w was determined using radiochemistry.

The rate and thermodynamic constants were taken from previous work. The values of k_5 and k_7 were calculated from their empirical dependence on temperature and salinity (Millero et al. 1987; Zhang and Millero 1993). The k_6 values ranging from 0.16 to 0.63 L mol^{-1} s^{-1} have been used for various coastal environments (Van Cappellen and Wang 1996; Berg et al. 2003). The k_8 values in previous work

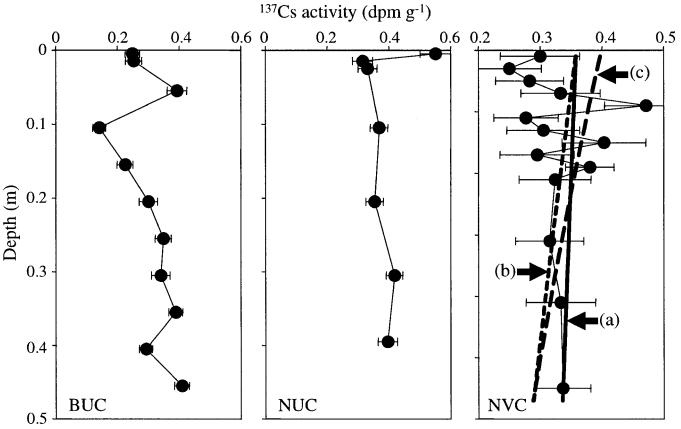

Fig. 1. Depth profiles of excess ^{137}Cs activities at BUC, NUC, and NVC. The ^{137}Cs profiles exhibited very little depth-dependent decreases for the sampling depths of the study. For NVC, the measured depth profile is plotted together with the calculated profiles according to Eq. (14). (a) The calculated profile with w = 10 cm yr^{-1}. (b) The calculated profile with w = 3 cm yr^{-1}. (c) The calculated profile with w = 2 cm yr^{-1}. A significant portion of the calculated profile for w = 2 cm yr^{-1} falls outside of the margin of error.

range from 1.3 × 10^{-4} to 7.0 × 10^{-4} L mol^{-1} s^{-1}, and k_9 ranges from 6.0 × 10^{-3} to 0.7 L mol^{-1} s^{-1} (Van Cappellen and Wang 1996; Boudreau et al. 1998; Berg et al. 2003). In the present study, the k_6, k_8, and k_9 values were taken from the highest values within these ranges, because the high temperature of the study site favored high rates. The pH-independent bimolecular rate expression for FeS precipitation, R_{10}, has only been tested recently in the arctic environment (Berg et al. 2003). A k_{10} value of 0.47 L mol^{-1} s^{-1} was used in this study. A higher value (4.7) was also tested but was found to have little effect on the modeled *kG*, C_{calc}, and TEA profiles. The value of k_N was taken from previous studies of costal fine-grained sediments (Mackin and Aller 1984). The carbon : nitrogen ratio of labile OM was taken from a recent study conducted at SERF (Gribsholt et al. 2003). The *Monod* constants were taken from previous work (Boudreau et al. 1998).

Radionuclide profiles and sediment accumulation rates—Activity profiles of ^{137}Cs (half-life, $T_{0.5}$ = 30.2 yr) from all stations lacked depth dependency (Fig. 1), which could be due to rapid sedimentation or intense bioturbation. Meanwhile, X-radiographs exhibited visible horizontal units, which indicates that bioturbation has not been intense enough to completely destroy sedimentary structures. Thus, the lack of depth dependency must be due to the rapid sedimentation. By applying the steady-state diffusion-decay equation,

$$D_B\frac{d^2C}{dx^2} - w\frac{dC}{dx} - \lambda C = 0 \tag{13}$$

where λ is the decay constant ($0.693/T_{0.5}$) to the ^{137}Cs profile from NVC, under the assumption that $D_B \approx 0$, one obtains the ^{137}Cs concentration as the function of depth,

$$[^{137}\mathrm{Cs}] = [^{137}\mathrm{Cs}]_{x=0}\exp\left(-\frac{\lambda x}{w}\right) \tag{14}$$

By applying the w values of 2, 3, and 10 cm yr^{-1} in Eq. 14, the modeled profiles (Fig. 1; NVC) are obtained. The [^{137}Cs]x = 0 value is adjusted for each case to seek a fit to the observed profile. The w value of 10 cm yr^{-1} yields a profile that is nearly independent of depth and fits most of the observed data points. Whereas w = 3 cm yr^{-1} yields a profile with some depth dependency, the modeled profile still falls within the counting errors of most of the data points. However, w = 2 cm yr^{-1} deviates further from the data points with more significant depth dependency. As a consequence, we used w values of 10 and 3 cm yr^{-1}. The effect of higher (i.e., 20 cm yr^{-1}) w value is also examined.

Burrow parameters and irrigation coefficient, α—The irrigation coefficient was estimated from the burrow observations using existing formulae (Koretsky et al. 2002) in which ecological measurements such as the number and size of burrows can be related to α as

$$\alpha = D_S\frac{S_v}{L} \tag{15}$$

S_v is the total burrow surface area divided by the total volume of sediments modeled for the given depth interval, and L is the radial diffusion length scale which is the difference between $\bar{r}$, the radial distance from the burrow axis at which the solute concentration reaches the radially averaged concentration for the bulk sediment at a given depth, and r_1, the equivalent burrow radius (Aller 1980; Boudreau 1984). The equivalent burrow radius is related to the total burrow surface area and density at a given depth in the equation

$$r_1(x) = \frac{\dfrac{\Delta S_v}{\Delta x}}{2\pi n_{tot}(x)} \tag{16}$$

where $n_{tot}(x)$ is the total number of burrows found at the given depth x within the unit area.

The values of L, S_v, n_{tot}, and r_1, as well as their depth dependency, are shown in Table 4 for all stations. The polychaete's contributions to S_v and n_{tot} were directly determined from the X-radiography data of burrow numbers, size, and tilt angles (Furukawa et al. 2001), whereas the contributions from *U. pugnax* were estimated by assuming that all *Uca* burrows observed at the WSI inside the 25 × 25 cm^2 quadrant had 1 depth extent of 0.2 m and a radius of 0.0075 m, which are the average depth (0.2 ± 0.025 m) and radius (0.0075 ± 0.0025 m) observed by previous studies (Teal 1958; Allen and Curran 1974; Basan and Frey 1977). The total S_v was simply the sum of polychaete and *Uca* contributions.

The value of L for *Uca* burrows was obtained by (1) assuming the radial O_2 penetration distance to be equal to L (Koretsky et al. 2002) and (2) averaging the direct measurements of radial O_2 penetration depths obtained along *Uca* burrows at the study site (0.82 × 10^{-3} [±3.3 × 10^{-4}] m). The radial O_2 penetration depth along polychaete burrows was not directly measured. The L ($\bar{r} - r_1$) value was instead

determined from the following ODE, boundary conditions, and an additional equation that assumed that D_S and the O_2 consumption rate (R) are identical between the sediments surrounding *Uca* burrows and surrounding polychaete burrows:

$$\frac{1}{r}\frac{d}{dr}\left(rD_s\frac{dC}{dr}\right) + R = 0,$$

$$C_{r=r_1} = C_0, \quad C_{r=\bar{r}} = 0, \quad \left.\frac{dC}{dr}\right|_{r=\bar{r}} = 0 \quad (17)$$

(Cai and Sayles 1996). For BUC, α was calculated separately for *Uca* and polychaetes, according to Eq. 15, before being added together to obtain the total α.

It is expected that phytoirrigation is important in the presence of *S. alterniflora*. However, the intensity of irrigation cannot be quantified using available data, because no information is currently available that links the intensity of phytoirrigation to the ecological data related to vegetation. As a consequence, α for NVC was derived using the burrow parameters in the same manner as for BUC and NUC, under the assumption that phytoirrigation is insignificant compared with the macrofaunal irrigation. The consequence of this assumption is discussed later.

Biodiffusion coefficient, D_B—We obtained estimated D_B values by assuming that the majority of particle displacement activity is due to the particle ingestion/egestion by macrofauna. The magnitude of particle ingestion/egestion has been found to be roughly proportional to the size of animals (Cammen 1980). The volumetric size of animals can be regarded as proportional to the cube of the burrow radius. In turn, the unit area-integrated burrow radius can be regarded as proportional to the cube of burrow surface area summed over all burrows divided by the total volume of sediments modeled within the given depth interval:

$$D_B = \gamma\delta_v^3$$

The value of scaling factor, γ, is adjusted so that D_B averaged for the top 10 cm of heavily bioturbated BUC falls within the empirically compiled D_B range of $10 < D_B < 1{,}000$ cm^2 yr^{-1} for bioturbated and rapidly accumulating sediments (Boudreau 1994). In practice, this meant that the value of γ was varied between 1.8×10^{-14} and 1.8×10^{-12}.

Depth-O_2 concentration profiles—The C_{measured} profiles for O_2 were obtained by combining measured vertical microprofiles at WSI and calculated effects of radial O_2 penetrations along burrow walls. The effect of radial penetration on the vertical profiles was determined by radially integrating the penetration profile perpendicular to the *Uca* burrows and averaging over the unit volume of sediments:

$$\bar{C} = N\int_{\bar{r}_i}^{\overline{r_i+L}} 2\pi C(r)\, dr \quad (19)$$

N is the number of burrows per unit lateral cross section area of sediments, $\bar{r}_1$ is the average burrow radius for the given depth, and $\overline{r_1 + L}$ is the average O_2 penetration radius. $C(r)$ is the function for the average radial O_2 concentration profile perpendicular to a burrow wall away from the WSI and is derived by solving Eq. 17 for C. The net vertical O_2 profiles were determined by combining the O_2 from vertical penetration, radial O_2 penetration along *Uca* burrows, and radial O_2 penetration along polychaete burrows. The polychaete burrow contribution was reduced to 20% of the values derived from Eq. 19, because polychaete irrigation is intermittent (Kristensen 2001). *Uca* burrows, with their large openings and simple geometry, were assumed to be fully oxygenated by bioirrigation and physical pumping.

Results

Inverse modeling yielded the *kG* profiles shown in Fig. 2. For each station, different D_B (i.e., different γ in Eq. 18; $\gamma = 1.8 \times 10^{-14}$, 1.8×10^{-13}, and 1.8×10^{-12}) and w (i.e., $w = 3$, 10, and 20 cm yr^{-1}) resulted in *kG* profiles that are similar. On the other hand, the comparison between stations reveals considerable differences. The OM degradation rate is modeled to be significantly higher at BUC and NVC than at NUC. The results also show that a major portion of OM at NUC is remineralized within ~1 cm of the WSI, whereas the remineralization occurs well below WSI at BUC and NVC, regardless of the parameter values chosen.

The inversely determined *kG* profiles were subsequently used in the forward modeling to calculate the depth-concentration profiles of major redox species and to confirm the agreement between measured and modeled profiles (Fig. 3). At BUC, the *kG* profiles calculated using the wide range of w (3, 10, and 20 cm yr^{-1}) yielded very similar C_{calc} profiles, whereas the choice of γ affected the results. The results show that $\gamma = 1.8 \times 10^{-12}$, which yields an average D_B for the top 10 cm at BUC of 1,000 cm^2 yr^{-1}, generates good agreement, whereas the smaller γ (i.e., smaller D_B) resulted in the modeled Fe-(oxy)hydroxide concentrations to reach zero within upper ~5 cm of sediments. The measurements indicate a significant presence of Fe-(oxy)hydroxides throughout the sampling depths. In NUC, the choice of w affected the calculated depth profiles whereas the choice of γ had negligible effect. Model calculations yielded reasonable agreement with the measured profiles when the low sedimentation rate ($w = 3$ cm yr^{-1}) was used in the calculations. Only the results using the *kG* profiles calculated with $w = 3$ cm yr^{-1} and $\gamma = 1.8 \times 10^{-12}$ are shown for NVC.

The forward model was also used to determine the depth profiles of OM degradation rate by each TEA, R_1, R_2, R_3, and R_4, according to the formulae in Table 2. The inversely determined *kG* profiles were used with the forward model-determined TEA concentrations in the formulae. Once these were determined, the rates of SO_4^{2-} and Fe(III)-(oxy)hydroxide consumption due to OM remineralization could be calculated as follows according to the reaction stoichiometry

$$R^{\text{OM}}_{SO_4^{2-}} = \frac{1-\varphi}{\varphi}\frac{1}{2}R \quad (\text{mol L-porewater}^{-1}\ \text{s}^{-1}) \quad (20)$$

$$R^{\text{OM}}_{Fe(OH)_3} = 4R_3 \quad (\text{mol dm}^{-3}\text{-solids s}^{-1}) \quad (21)$$

The $R^{\text{OM}}_{Fe(OH)_3}$ and $R^{\text{OM}}_{SO_4^{2-}}$ profiles are plotted in Fig. 4, together

Table 4. Burrow parameter summary.

	BUC									
	Uca				Polychaete				Total	
Depth (m)	Density n_{Uca} (m^{-2})	Radius r_{1Uca} (m)	Burrow surface area DSv/Dx (m)	Diffusion length scale L (m)	Density n_{poly} (m^{-2})	Radius r_{1poly} (m)	Burrow surface area DSv/Dx (m)	Diffusion length scale L (m)	Burrow surface area DSv/Dx (m)	$(DSv/L)_{Uca} + (DSv/L)_{poly}$
0.00	131	0.0075	6.17	7.00×10^{-4}	713	5.58×10^{-4}	2.50	5.05×10^{-4}	8.67	13,763
0.01	131	0.0075	6.17	7.00×10^{-4}	713	5.58×10^{-4}	2.50	5.05×10^{-4}	8.67	13,763
0.02	131	0.0075	6.17	7.00×10^{-4}	446	7.89×10^{-4}	2.21	5.45×10^{-4}	8.38	12,866
0.03	131	0.0075	6.17	7.00×10^{-4}	357	5.62×10^{-4}	1.26	5.06×10^{-4}	7.43	11,303
0.04	131	0.0075	6.17	7.00×10^{-4}	178	9.04×10^{-4}	1.01	5.60×10^{-4}	7.18	10,615
0.05	131	0.0075	6.17	7.00×10^{-4}	267	1.01×10^{-3}	1.69	5.71×10^{-4}	7.86	11,769
0.06	131	0.0075	6.17	7.00×10^{-4}	891	1.05×10^{-3}	5.85	5.75×10^{-4}	12.02	18,986
0.07	131	0.0075	6.17	7.00×10^{-4}	980	8.56×10^{-4}	5.27	5.54×10^{-4}	11.44	18,325
0.08	131	0.0075	6.17	7.00×10^{-4}	446	8.03×10^{-4}	2.25	5.47×10^{-4}	8.42	12,925
0.09	131	0.0075	6.17	7.00×10^{-4}	535	1.07×10^{-3}	3.59	5.77×10^{-4}	9.76	15,031
0.10	131	0.0075	6.17	7.00×10^{-4}	178	7.60×10^{-4}	0.85	5.41×10^{-4}	7.02	10,382
0.11	131	0.0075	6.17	7.00×10^{-4}	89	5.55×10^{-4}	0.31	5.04×10^{-4}	6.48	9,426
0.12	131	0.0075	6.17	7.00×10^{-4}	624	8.70×10^{-4}	3.41	5.56×10^{-4}	9.58	14,948
0.13	131	0.0075	6.17	7.00×10^{-4}	267	6.80×10^{-4}	1.14	5.28×10^{-4}	7.31	10,970
0.14	131	0.0075	6.17	7.00×10^{-4}	267	5.96×10^{-4}	1.00	5.13×10^{-4}	7.17	10,761
0.15	131	0.0075	6.17	7.00×10^{-4}	357	9.77×10^{-4}	2.19	5.68×10^{-4}	8.36	12,667
0.16	131	0.0075	6.17	7.00×10^{-4}	535	1.89×10^{-3}	6.35	6.28×10^{-4}	12.52	18,914
0.17	131	0.0075	6.17	7.00×10^{-4}	178	7.96×10^{-4}	0.89	5.46×10^{-4}	7.06	10,441
0.18	131	0.0075	6.17	7.00×10^{-4}	178	6.71×10^{-4}	0.75	5.26×10^{-4}	6.92	10,235
0.19	131	0.0075	6.17	7.00×10^{-4}	178	8.05×10^{-4}	0.90	5.47×10^{-4}	7.07	10,455
0.20	131	0.0075	6.17	7.00×10^{-4}	178	5.10×10^{-4}	0.57	4.94×10^{-4}	6.74	9,965

with the experimentally measured SRR values. The measured SRR is expressed in terms of mol L pore water^{-1} s^{-1}, to allow a direct comparison with the model-calculated R^{OM2}_{SO4}. For BUC, the measured SRR and model-calculated R^{OM2}_{SO4} are in agreement. Model-calculated R^{OM2}_{SO4} profiles would be three to four times greater if the smaller γ values were used, generating poor agreement with the measured SRR. The model-calculated R^{OM2}_{SO4} profile is smaller than measured SRR for NUC. For NVC, the net R^{OM2}_{SO4} and SRR for the upper 9 cm of the sediments are in general agreement, although the depth-dependent fluctuation found in the model results was not observed in the field.

The relative importance of Fe(III)-(oxy)hydroxides as a TEA was calculated to be greater at the heavily bioturbated BUC than at NUC or NVC (Fig. 5). At NUC and NVC, model results show that SO_4^{2-} is responsible for the majority of OM degradation. In contrast, a significant fraction of OM degradation proceeds via reduction of Fe(III)-(oxy)hydroxides at BUC.

Discussion

Effect of macrobenthos on kG—The model results indicate that macrobenthos affect the chemical mass transfer in Skidaway SERF sediments. A comparison of BUC and NUC profiles (Fig. 2) illustrates the effect of bioturbation. The net rate of OM degradation is much greater (~8 times) in the bioturbated sediments of BUC than in NUC. In addition, most of the OM degradation occurs within the immediate vicinity of WSI in NUC, whereas it takes place well into the deeper part of the sediments in BUC. Although the observed lack of SO_4^{2-} and $Fe(OH)_3$ depletion at BUC (Fig. 3) may suggest a lack of significant OM degradation, the modeling, with its forcing of the high rate of biological transport, reveals the reason for the lack of TEA depletion. TEAs penetrate deeper at BUC not because they are underutilized but because they are transported and regenerated.

The comparison of *kG* profiles from NUC and NVC (Fig. 2) makes clear that vegetation also enhances the sedimentary OM degradation rates: the net OM degradation is greater (~14 times) in the heavily vegetated sediments of NVC than in NUC. In addition, OM degradation takes place well into the deeper part of the sediments in NVC, whereas it is restricted to the immediate vicinity of WSI in NUC.

Parameter selections—We examined a range of sediment accumulation rates (w) and scaling factors for the biodiffusion coefficient (γ). Appropriate values for these parameters may be selected by comparing the model results with the measurements from this and previous studies. A recent study within SERF at a bioturbated station similar to BUC has shown that, at the depth of 5 cm, >50% of OM remineralization occurs through the reduction of Fe(III) minerals (Gribsholt et al. 2003). The model-calculated relative importance of TEAs at BUC agrees with this result, showing that ~50% of the OM degradation proceeds through $Fe(OH)_3$ reduction at 5–6 cm below WSI (Fig. 5). The lower γ values, $\gamma = 1.8 \times 10^{-14}$ and 1.8×10^{-13}, would decrease

Table 4. Extended.

NUC				NVC			
Polychaete				Polychaete			
Density n_{poly}	Radius r_{1poly}	Burrow surface area DSv/Dx (m)	Diffision length scale L (m)	Denstiy n_{poly}	Radius r_{1poly}	Burrow surface area DSv/Dx (m)	Diffusion length scale L (m)
201	5.78×10^{-4}	0.73	5.09×10^{-4}	446	5.63×10^{-4}	1.57	5.06×10^{-4}
201	5.78×10^{-4}	0.73	5.09×10^{-4}	446	5.63×10^{-4}	1.57	5.06×10^{-4}
334	9.12×10^{-4}	1.92	5.61×10^{-4}	1070	1.02×10^{-3}	6.87	5.73×10^{-4}
67	6.85×10^{-4}	0.29	5.29×10^{-4}	1693	7.78×10^{-4}	8.27	5.43×10^{-4}
67	5.00×10^{-4}	0.21	4.91×10^{-4}	1337	7.80×10^{-4}	6.55	5.44×10^{-4}
134	5.23×10^{-4}	0.44	4.97×10^{-4}	802	8.24×10^{-4}	4.15	5.50×10^{-4}
401	8.16×10^{-4}	2.05	5.49×10^{-4}	1426	1.01×10^{-3}	9.09	5.72×10^{-4}
334	6.35×10^{-4}	1.33	5.20×10^{-4}	624	1.15×10^{-3}	4.51	5.85×10^{-4}
201	1.57×10^{-3}	1.98	6.13×10^{-4}	267	7.06×10^{-4}	1.19	5.32×10^{-4}
267	8.28×10^{-4}	1.39	5.50×10^{-4}	267	8.26×10^{-4}	1.39	5.50×10^{-4}
67	5.18×10^{-4}	0.22	4.96×10^{-4}	624	9.50×10^{-4}	3.72	5.65×10^{-4}
0		0.00		446	3.15×10^{-3}	8.80	6.63×10^{-4}
0		0.00		178	6.07×10^{-4}	0.68	5.15×10^{-4}
0		0.00		267	7.81×10^{-4}	1.31	5.44×10^{-4}
0		0.00		267	7.42×10^{-4}	1.25	5.38×10^{-4}
0		0.00		446	1.08×10^{-3}	3.03	5.78×10^{-4}
0		0.00		267	5.32×10^{-4}	0.89	4.99×10^{-4}
0		0.00		446	9.82×10^{-4}	2.75	5.69×10^{-4}
0		0.00		0		0.00	
134	7.06×10^{-4}	0.59	5.32E-04	0		0.00	
134	5.03×10^{-4}	0.42	4.92E-04	89	1.39×10^{-3}	0.78	6.02×10^{-4}

the relative importance of $Fe(OH)_3$ in this depth interval to ~0% and 3%, respectively. The comparison of model-calculated and measured SRRs (Fig. 4) reveals that measured SRR at BUC are reasonably matched by using $\gamma = 1.8 \times 10^{-12}$. Moreover, the comparison of concentration profiles at BUC (Fig. 3) shows that the modeling with a smaller D_B (i.e., $\gamma = 1.8 \times 10^{-14 \sim -13}$) would result in the exhaustion of Fe(III)-(oxy)hydroxides within the upper ~5 cm of sediments, even though significant amount is observed throughout the sampling depth. Thus, $\gamma = 1.8 \times 10^{-12}$ is likely the most appropriate choice.

The forward-model simulations of concentration profiles using the high sediment accumulation rate values (i.e., 10 and 20 cm yr^{-1}; Fig. 3) result in the deeper penetration of Fe(III)-(oxy)hydroxides in comparison to the directly measured profiles at NUC. Thus, the w values of 3 cm yr^{-1} are likely the more appropriate choice.

The combined use of $w = 3$ cm yr^{-1} and $\gamma = 1.8 \times 10^{-12}$ yields agreement between measured and modeled concentration profiles at all stations (Fig. 3). There is reasonable agreement between measured and model-calculated SRR for BUC. The depth-integrated measured SRR and modeled $R^{OM2-}_{SO\,4}$ for the upper 9 cm of sediments are calculated as follows:

$$\Sigma R_{SO_4^{2-}} = 10^3 \varphi \int_0^{0.09} R^{OM}_{SO_4^{2-}}\, dx \quad (\text{mol m}^{-2}\ \text{s}^{-1}) \qquad (22)$$

The results, shown in Table 5, are comparable for BUC and NVC.

Effect of C : N ratio in NUC—The NUC modeling results exhibit the underestimation of $R^{OM2-}_{SO\,4}$ compared with the measured SRR (Fig. 4). Also, the forward modeling reveals that the simultaneous agreement between measured and model-calculated concentration profiles is not achieved for NUC as SO_4^{2-} is overestimated by the model (Fig. 3). This discrepancy may be due to the model use of an inappropriately low C : N ratio. A low C : N ratio in the NH_4^+ profile matching processes of inverse modeling would result in the underestimation of kG, which would lead to the underestimation of $R^{OM2-}_{SO\,4}$. Given the lack of fresh OM input from vegetation and bioturbation, the penetration of labile, N-rich OM is limited at NUC except, for the immediate vicinity of WSI. The decomposing *Spartina* plants, whose C : N ratio has been reported to be 32–54 at nearby Sapelo Island (Haines et al. 1977), would result in a high C : N ratio in the absence of more labile, N-rich OM. By using the high end value of C : N = 54 instead of 12.5 at NUC in conjunction with $w = 3$ cm yr^{-1} and $\gamma = 1.8 \times 10^{-12}$, we obtained forward-model results (Fig. 6) in which the agreement between measured and model-calculated profiles was improved. The simulation with C : N = 54 also yielded an improved match between measured SRR and model-calculated $R^{OM2-}_{SO\,4}$ (Fig. 7, Table 5). The depth-integrated SRR at NUC using the adjusted C : N were also comparable to the values measured in August 2000 at a *Uca*- and *Spartina*-free part of the Skidaway SERF (Kostka et al. 2002*a*).

The improved agreement suggests that the C : N ratio of degrading OM at NVC is likely to be closer to 54 than to

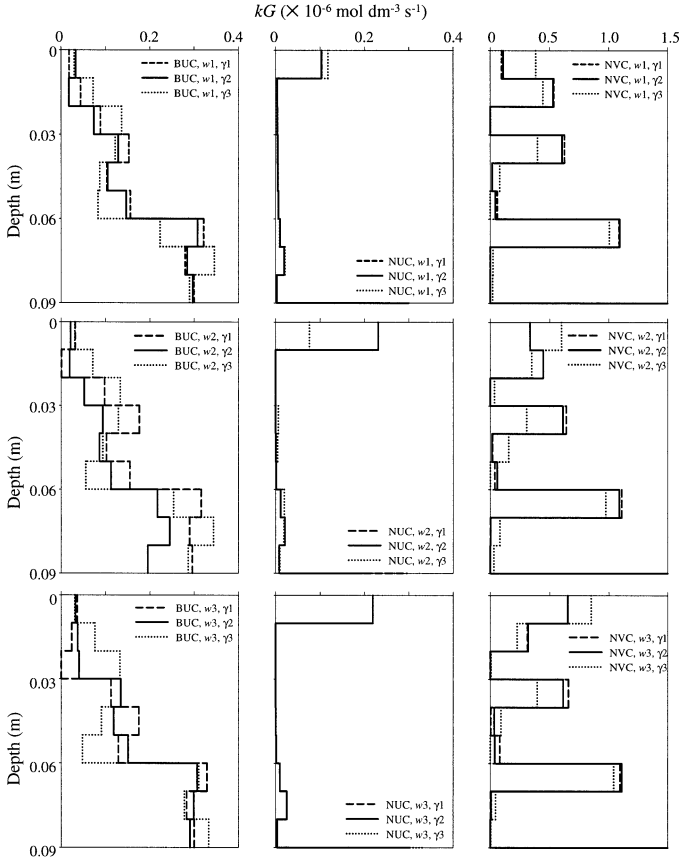

Fig. 2. The model-calculated depth profiles of OM degradation rate (kG) for BUC, NUC, and NVC. In the legends, $w1$, $w2$, and $w3$ denote model runs using w = 3, 10, and 20 (cm yr^{-1}), respectively, and $\gamma 1$, $\gamma 2$, and $\gamma 3$ represent runs with $\gamma = 1.8 \times 10^{-14}$, 1.8×10^{-13}, and 1.8×10^{-12}, respectively. At NUC, the OM degradation is fastest in the immediate vicinity of WSI (0–0.01 m) than in the deeper part of the sediments. On the other hand, at BUC and NVC, the OM degradation occurs in the deeper parts of the sediments, and the net OM degradation is greater than NUC.

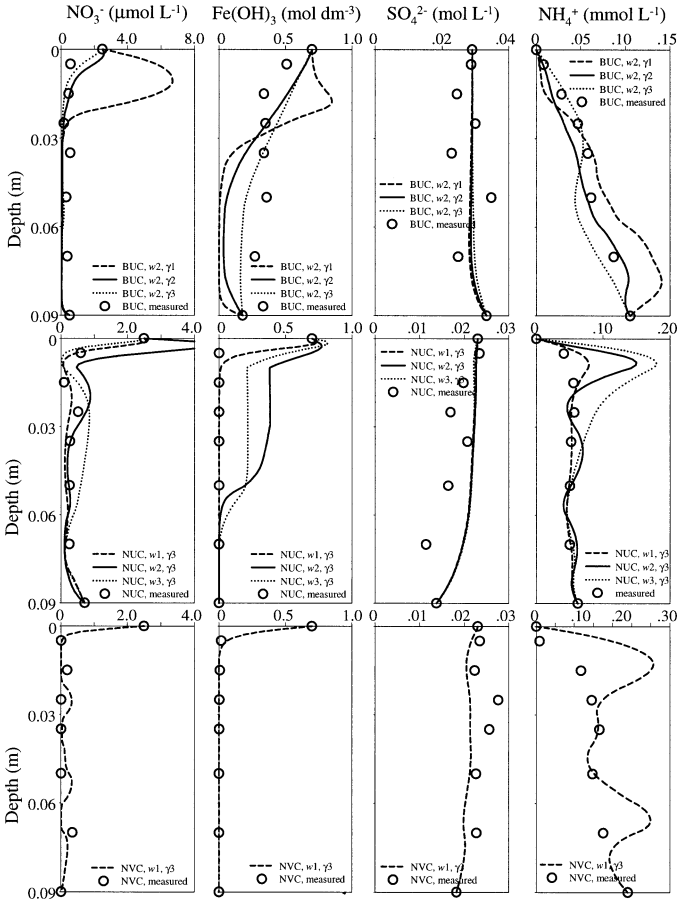

Fig. 3. The comparison of model-calculated and measured concentration-depth profiles of major redox species. For BUC, different γ values yielded different results, as shown. For NUC, the selection of sediment accumulation rates (w) affected the calculation results, as shown.

12.5. The C : *N* ratio of remineralizing OM is different from the bulk C : *N* ratio in any given sample (Berg et al. 2003), and there is no direct method that can quantify the C : *N* ratio of degrading OM in situ. The parameter fitting approach taken here can be a reasonable method when one needs to determine the C : *N* ratio of degrading OM.

Integrated TEA utilization rates versus TEA fluxes—TEA utilization rate profiles can be used to calculate the net, integrated TEA utilization rates for the upper 9 cm of sediments at BUC, NUC, and NVC. For $Fe(OH)_3$,

$$\Sigma R_{\mathrm{Fe(III)}} = 10^3(1 - \varphi) \int_0^{0.09} R^{\mathrm{OM}}_{\mathrm{Fe(III)}}\, dx \quad (\mathrm{mol\ m^{-2}\ s^{-1}}) \qquad (23)$$

The value for each station is shown in Table 5. The integrated value at BUC is comparable to 4.0×10^{-6} mol m^{-2} s^{-1}, the value found previously by an incubation for a bioturbated and vegetated substation in SERF (Kostka et al. 2002*a*). The flux of Fe(III)-(oxy)hydroxides to the SERF sediments, $F_{\mathrm{Fe(III)}}$ mol m^{-2} s^{-1}, can be estimated from the total solid-phase iron, ΣFe (moles dm^{-3}-solids), and sediment accumulation rates, w (m s^{-1}), as follows:

$$F_{\mathrm{Fe(III)}} = 10^3 w(1 - \varphi)\, \Sigma\mathrm{Fe} \qquad (24)$$

where ΣFe is the total solid-phase iron (= Fe(III) + Fe(II)) averaged for the entire depth of sediment columns studied. The directly measured ΣFe are similar at all three stations (i.e., $\Sigma\mathrm{Fe} \approx 0.7$ moles L-solids^{-1}). Consequently, the flux of Fe(III)-(oxy)hydroxides to either station is the function of w and φ, and the value, nearly identical for all stations, is shown in Table 5.

The comparison of $\Sigma R_{\mathrm{Fe(III)}}$ and $F_{\mathrm{Fe(III)}}$ reveals that, at NUC, the flux of Fe(III)-(oxy)hydroxide due to sediment accumulation is closely matched by the calculated cumulative rate of its consumption because of OM degradation within upper 9 cm of the sediments. The lack of Fe recycling in turn increases the relative importance of SO_4^{2-} as the TEA. A recent study at a *Uca*- and *Spartina*-free part of the Skidaway SERF found that >70% of OM remineralization was through the reduction of SO_4^{2-} (Kostka et al. 2002*a*). At NVC, the integrated Fe(III) consumption rate is also similar to the flux.

In contrast, at BUC, the calculated cumulative consump-

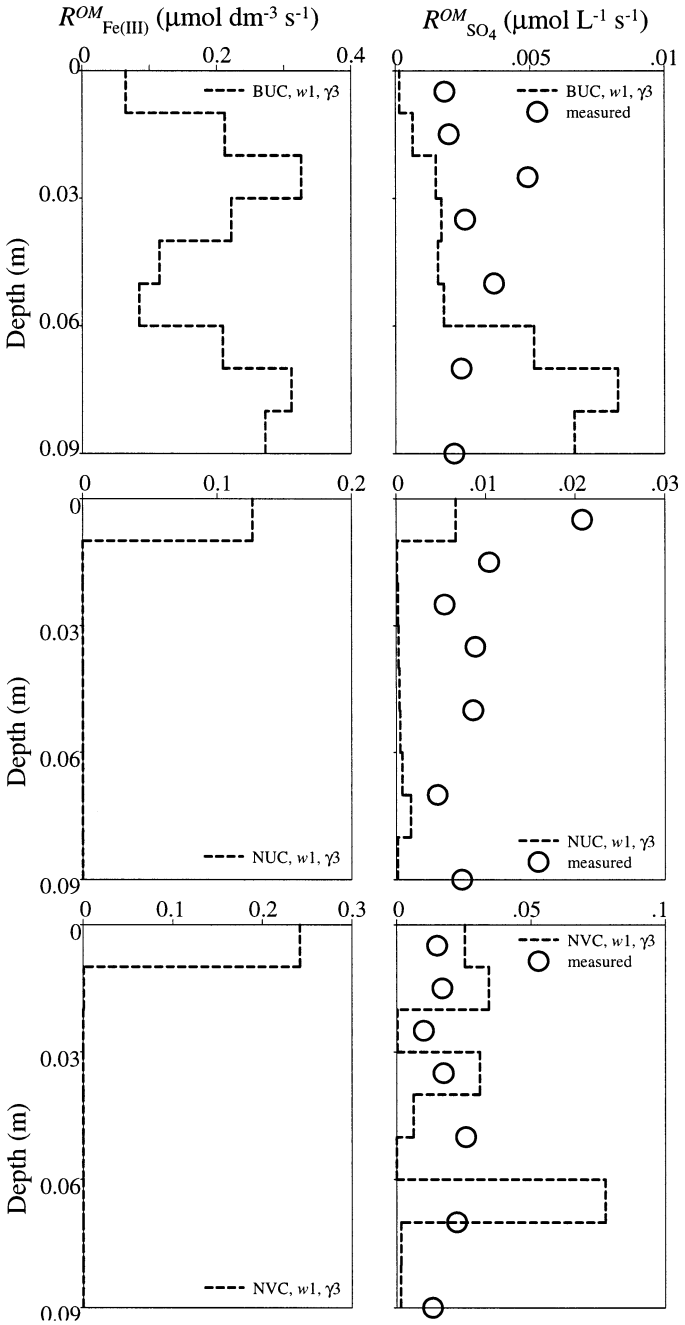

Fig. 4. Model-calculated depth profiles of Fe(III)-(oxy)hydroxide reduction rates and SO_4^{2-} reduction rates caused by OM remineralization. The measured SRR profiles are also plotted for comparison. It should be noted that SRR is expressed in terms of the rate of SO_4^{2-} consumption in the unit volume of pore water (μmol L^{-1} s^{-1}). For BUC, the choice of smaller γ values ($\gamma = 1.8 \times 10^{-14}$ and 1.8×10^{-13}) resulted in the SO_4^{2-} reduction rate that is three to four times greater than the measured SRR.

tion rate of Fe(III)-(oxy)hydroxides in the upper 9 cm of sediments is 30 times greater than the flux, which suggests that each Fe atom experiences cycling between reducing and oxidizing environments at least ~30 times via bioturbation before it is permanently buried below the zone of biological mixing. This value is underestimating the magnitude of recycling, because the zone of biological mixing at BUC is >9 cm (Table 4). This significant recycling results in the enhanced relative importance of Fe(III) as a TEA at BUC. The rate expression for $Fe(OH)_3$ production (Table 2) indicates that it depends on one reaction, the aerobic oxidation of Fe^{2+} (i.e., R_5). The high bioturbation and irrigation rates are the key to maintaining the deep penetration of O_2 that allows the continuous production of $Fe(OH)_3$. The Fe recycling of ~30 times is approaching the value of 100~300 determined in the shallow marine environment of Skagerrak off the coast of Denmark (Canfield et al. 1993). Meanwhile, in sediments with limited particle mixing (i.e., NUC and NVC), solid-phase TEAs such as Fe(III)-(oxy)hydroxides are reduced once and are not reoxidized to participate in repeated reduction.

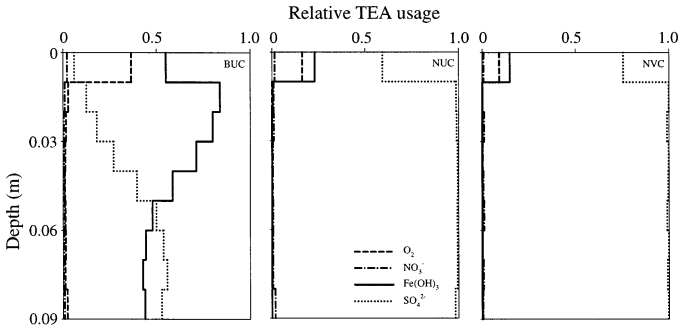

Fig. 5. The relative importance of O_2, NO_3^-, Fe(III), and SO_4^{2-} as TEAs in the OM remineralization, plotted as a function of depth. These were calculated by normalizing the model-calculated R_1, R_2, R_3, or R_4 by ($R_1 + R_2 + R_3 + R_4$).

The model provides independent confirmation that bioturbation drives particle and solute mixing at BUC. Previous experimental studies (Thamdrup 2000; Kostka et al. 2002*a*,*b*; Gribsholt et al. 2003) have indicated that Fe(III) respiration is sustained by metal oxides supplied via bioturbation. Because Fe(III) minerals becomes less reactive with age after precipitation, it may also be speculated that rapid recycling due to bioturbation keeps Fe(III) minerals in a poorly crystalline state, exerting a positive feedback on microbial Fe(III) respiration (Thamdrup 2000). This positive feedback would also support the enhanced OM degradation rates under redox-oscillating environments (Aller 1994).

Effects of phytoirrigation—To examine whether phytoirrigation is quantitatively significant for the transport of major solute species, additional model runs were conducted for NVC. It should be noted that the elevated α would affect all species equally and would not simulate the uptake of specific solute species. One simulation was conducted with the depth-independent α whose value was derived by first taking the average, macrofauna-only α values for each species in the upper 10 cm of NVC sediments, and increasing it by three times. Another simulation was conducted by using ten times the average, macrofauna-only α value. The model-calculated $R^{OM2-}_{SO\,4}$ profiles using the elevated α values significantly overestimate the measured SRR values at NVC, which indicates that the elevated α values do not appropriately depict the irrigation in NVC. This implies that the net

Table 5. Comparison of depth-integrated measured SRR and model-calculated $R^{OM}_{SO_4^{2-}}$, as well as the depth-integrated Fe(III) flux and model-calculated $R^{OM}_{Fe(OH)_3}$ for the upper 0.09 m of sediments. The consumption rates were determined by the model using the parameter values of $w = 3$ cm yr^{-1} and $\gamma = 1.8 \times 10^{-12}$, whereas the flux was estimated from the measured total iron concentrations and sediment accumulation rate ($w = 3$ cm yr^{-1}).

	BUC (mol m^{-2} s^{-1})	NUC (mol m^{-2} s^{-1})		NVC (mol m^{-2} s^{-1})
		C:N = 12.5	C:N = 54	
Measured SRR	1.5×10^{-7}	4.8×10^{-7}		9.6×10^{-7}
Model-calculated $R^{OM}_{SO_4^{2-}}$	2.3×10^{-7}	0.9×10^{-7}	4.5×10^{-7}	15.3×10^{-7}
$\Sigma R_{Fe(III)}$ (mol m^{-2} s^{ms1})	2.7×10^{-6}	1.9×10^{-7}	1.4×10^{-7}	3.6×10^{-7}
$F_{Fe(III)}$ (mol m^{-2} s^{-1})		9×10^{-8} (constant for all stations)		
$\Sigma R/F$	30	2.1	1.6	4.0

transport of the solute species by *Spartina* root systems may not be quantitatively significant, compared with the transport by small amount of polychaete bioirrigation in the vegetated portion of the study site.

Although phytoirrigation appears to be insignificant as a net solute transport mechanism, the effect of vegetation in the salt marsh chemical mass transfer is important. The comparison of *kG* profiles between NUC and NVC (Fig. 2) makes it evident that the vegetation significantly enhances the net OM degradation rate. The remineralization of OM occurs predominantly in the immediate vicinity of WSI at NUC in the absence of *Spartina* plants, whereas it occurs throughout the sampling depths at NVC. Both model-calculated and measured SO_4^{2-} reduction rates show the depth-dependent decrease in SO_4^{2-} reduction rates at NUC and depth-independent, quantitatively significant amount of SO_4^{2-} reduction throughout the sampling depth at NVC (Fig. 4). It can be speculated that *Spartina* root systems enhance microbial activities by modifying the habitats through the influx of O_2, labile OM, and nutrients, as well as through the removal of toxic metabolites and metals. The current modeling has limited utility in phytoirrigation study, because it does not explicitly account for the preferential uptake of certain solute species. Such an account would require a better understanding of the chemical mass transfer by *Spartina* root systems. Further investigations of the concentrations, activity, and spatial distribution of various geochemical species and microorganisms in relation to the root system geometry are warranted.

In summary, the rates of OM remineralization and TEA consumptions were determined for the bioturbated and vegetated salt marsh sediments of the Skidaway SERF using the inverse modeling. The models were constrained by the ecological data as well as measured concentration profiles of major redox species, and the model results were verified by the measured depth profiles of SRR. The agreement between measured and modeled profiles indicates that the a priori parameter values, including those associated with the bioturbation and irrigation, are reasonable. The calculated rate profiles not only reveal the difference in the net OM degradation rates between stations but also verify the significant difference in the relative importance of Fe(III)-(oxy)hydroxides and SO_4^{2-} as TEAs between stations with varying degrees of bioturbation. In heavily bioturbated BUC, Fe(III)-(oxy)hydroxides are recycled ≥30 times before they are permanently buried below the zone of bioturbation. Recycling at NUC and NVC, the stations that host few bioturbating organisms, is limited to only a few times. The model results also confirm the significance of vegetation in salt marsh chemical mass transfer. Although the phytoirrigation

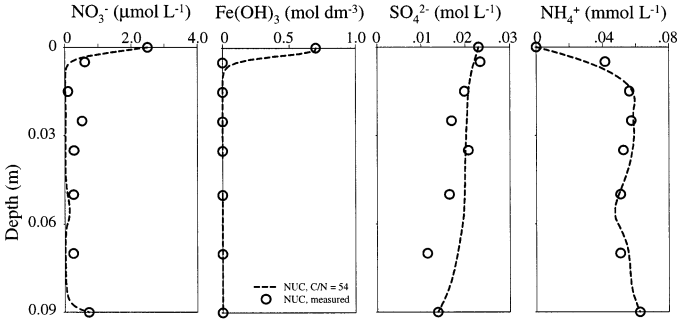

Fig. 6. For NUC, an elevated C : *N* ratio (54) yields model-calculated depth-concentration profiles that agree well with the measured profiles.

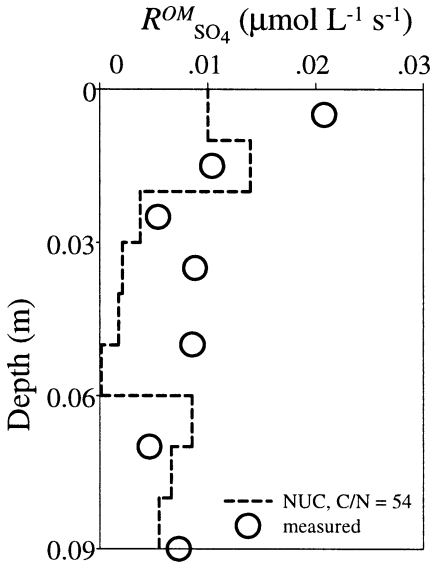

Fig. 7. For NUC, an elevated C : *N* ratio (54) yields model-calculated SO_4^{2-} reduction rate profile that is comparable to the measured SRR.

of major solute species appears to be insignificant, *Spartina* root systems enhance the rate of OM remineralization in subsurface sediments well away from WSI, where labile OM and microbial activities may otherwise be limited.

References

ALEXANDER, C. R., D. J. DEMASTER, AND C. A. NITTROUER. 1991. Sediment accumulation in a modern epicontinental shelf setting—the Yellow Sea. Mar. Geol. **98:** 51–72.

ALLEN, E. A., AND H. A. CURRAN. 1974. Biogenic sedimentary structures produced by crabs in lagoon margin and salt marsh environments near Beaufort, North Carolina. J. Sediment. Petrol. **44:** 538–548.

ALLER, R. C. 1980. Quantifying solute distributions in the bioturbated zone of marine sediments by defining an average micro environment. Geochim. Cosmochim. Acta **44:** 1955–1965.

———. 1994. Bioturbation and remineralization of sedimentary organic-matter—effects of redox oscillation. Chem. Geol. **114:** 331–345.

ARCHER, D. E., J. L. MORFORD, AND S. R. EMERSON. 2002. A model of suboxic sedimentary diagenesis suitable for automatic tuning and gridded global domains. Global Biogeochem. Cycles **16:** 1017. doi:10.1029/2000GB001288

BASAN, P. B., AND R. W. FREY. 1977. Actual-palaeontology and neoichnology of salt marshes near Sapelo Island, Georgia, p. 41–70. *In* T. P. Crimes and J. C. Harper [eds.], Trace fossils 2, Geological Journal, special issue. Seel House.

BERG, P., N. RISGAARD-PETERSEN, AND S. RYSGAARD. 1998. Interpretation of measured concentration profiles in sediment pore water. Limnol. Oceanogr. **43:** 1500–1510.

———, S. RYSGAARD, AND B. THAMDRUP. 2003. Dynamic modeling of early diagenesis and nutrient cycling. A case study in an Arctic marine sediment. Am. J. Sci. **303:** 905–955.

BERNER, R. A. 1980. Early diagenesis: A theoretical approach. Princeton Univ. Press.

BOUDREAU, B. P. 1984. On the equivalence of nonlocal and radial diffusion models for porewater irrigation. J. Mar. Res. **42:** 731–735.

———. 1994. Is burial velocity a master parameter for bioturbation. Geochim. Cosmochim. Acta **58:** 1243–1249.

———. 1996*a*. Diagenetic models and their implementation: modelling transport and reaction in aquatic sediments. Springer-Verlag.

———. 1996*b*. A method-of-lines code for carbon and nutrient diagenesis in aquatic sediments. Comput. Geosci. **22:** 479–496.

———, A. MUCCI, B. SUNDBY, G. W. LUTHER, AND N. SILVERBERG. 1998. Comparative diagenesis at three sites on the Canadian continental margin. J. Mar. Res. **56:** 1259–1284.

CAI, W. J., AND F. L. SAYLES. 1996. Oxygen penetration depths and fluxes in marine sediments. Mar. Chem. **52:** 123–131.

CAMMEN, L. M. 1980. Ingestion rate—empirical-model for aquatic deposit feeders and detritivores. Oecologia **44:** 303–310.

CANFIELD, D. E., B. THAMDRUP, AND J. W. HANSEN. 1993. The anaerobic degradation of organic matter in Danish coastal sediments—iron reduction, manganese reduction, and sulfate reduction. Geochim. Cosmochim. Acta **57:** 3867–3883.

CHILDERS, D. L., S. COFERSHABICA, AND L. NAKASHIMA. 1993. Spatial and temporal variability in marsh water column interactions in a southeastern USA salt-marsh estuary. Mar. Ecol. Prog. Ser. **95:** 25–38.

COLEMAN, T. F., AND Y. Y. LI. 1996. An interior trust region approach for nonlinear minimization subject to bounds. Siam J. Optimiz. **6:** 418–445.

CUTSHALL, N. H., I. L. LARSEN, AND C. R. OLSEN. 1983. Direct analysis of Pb-210 in sediment samples—self-absorption corrections. Nucl. Instrum. Methods **206:** 309–312.

FOSSING, H., AND B. B. JØRGENSEN. 1989. Measurement of bacterial sulfate reduction in sediments—evaluation of a single-step chromium reduction method. Biogeochemistry **8:** 205–222.

FROELICH, P. N., AND OTHERS. 1979. Early oxidation of organic-matter in pelagic sediments of the eastern equatorial Atlantic—suboxic diagenesis. Geochim. Cosmochim. Acta **43:** 1075–1090.

FURUKAWA, Y. 2001. Biogeochemical consequences of macrofauna burrow ventilation. Geochem. Trans. **2:** 83–91.

———, S. J. BENTLEY, AND D. L. LAVOIE. 2001. Bioirrigation modeling in experimental benthic mesocosms. J. Mar. Res. **59:** 417–452.

GLUD, R. N., J. K. GUNDERSEN, AND N. B. RAMSING. 2000. Electrochemical and optical oxygen microsensors for in situ measurements, p. 19–73. *In* J. Buffle and G. Horvai [eds.], In situ monitoring of aquatic systems: Chemical analysis and speciation. Wiley.

GONI-URRIZA, M., X. DE MONTAUDOUIN, R. GUYONEAUD, G. BACHELET, AND R. DE WIT. 1999. Effect of macrofaunal bioturbation on bacterial distribution in marine sandy sediments, with special reference to sulphur-oxidising bacteria. J. Sea Res. **41:** 269–279.

GRIBSHOLT, B., J. E. KOSTKA, AND E. KRISTENSEN. 2003. Impact of fiddler crabs and plant roots on sediment biogeochemistry in a Georgia saltmarsh. Mar. Ecol. Prog. Ser. **259:** 237–251.

HAINES, E., A. CHALMERS, R. HANSON, AND B. SHERR. 1977. Nitrogen pools and fluxes in a Georgia salt marsh, p. 241–254. *In* E. Wiley [ed.], Estuarine processes. Academic.

HERBERT, R. A. 1999. Nitrogen cycling in coastal marine ecosystems. FEMS Microbiol. Rev. **23:** 563–590.

HOWARTH, R. W., AND A. GIBLIN. 1983. Sulfate reduction in the salt marshes at Sapelo Island, Georgia. Limnol. Oceanogr. **28:** 70–82.

KING, G. M. 1988. Patterns of sulfate reduction and the sulfur cycle in a South-Carolina salt-marsh. Limnol. Oceanogr. **33:** 376–390.

KORETSKY, C. M., C. MEILE, AND P. VAN CAPPELLEN. 2002. Quantifying bioirrigation using ecological parameters: A stochastic approach. Geochem. Trans. **17–30:** 83–91.

———, C. M. MOORE, K. L. LOWE, C. MEILE, T. J. DICHRISTINA, AND P. VAN CAPPELLEN. 2003. Seasonal oscillation of microbial iron and sulfate reduction in saltmarsh sediments (Sapelo Island, GA, USA). Biogeochemistry **64:** 179–203.

KOSTKA, J. E., B. GRIBSHOLT, E. PETRIE, D. DALTON, H. SKELTON, AND E. KRISTENSEN. 2002*a*. The rates and pathways of carbon oxidation in bioturbated saltmarsh sediments. Limnol. Oceanogr. **47:** 230–240.

———, A. ROYCHOUDHURY, AND P. VAN CAPPELLEN. 2002*b*. Rates and controls of anaerobic microbial respiration across spatial and temporal gradients in saltmarsh sediments. Biogeochemistry **60:** 49–76.

KRISTENSEN, E. 2001. Impact of polychaetes (*Nereis spp.* and *Arenicola marina*) on carbon biogeochemistry in coastal marine sediments. Geochem. Trans. **2:** 92–103.

———, M. H. JENSEN, AND R. C. ALLER. 1991. Direct measurement of dissolved inorganic nitrogen exchange and denitrification in individual polychaete (*Nereis virens*) burrows. J. Mar. Res. **49:** 355–377.

LOWE, K. L., T. J. DICHRISTINA, A. N. ROYCHOUDHURY, AND P. VAN CAPPELLEN. 2000. Microbiological and geochemical characterization of microbial Fe(III) reduction in salt marsh sediments. Geomicrobiol. J. **17:** 163–176.

LUTHER, G. W., T. M. CHURCH, J. R. SCUDLARK, AND M. COSMAN.

1986. Inorganic and organic sulfur cycling in salt-marsh pore waters. Science **232:** 746–749.

MACKIN, J. E., AND R. C. ALLER. 1984. Ammonium adsorption in marine sediments. Limnol. Oceanogr. **29:** 250–257.

MARINELLI, R. L., C. R. LOVELL, S. G. WAKEHAM, D. B. RINGELBERG, AND D. C. WHITE. 2002. Experimental investigation of the control of bacterial community composition in macrofaunal burrows. Mar. Ecol. Prog. Ser. **235:** 1–13.

MEILE, C., C. M. KORETSKY, AND P. VAN CAPPELLEN. 2001. Quantifying bioirrigation in aquatic sediments: An inverse modeling approach. Limnol. Oceanogr. **46:** 164–177.

MIDDELBURG, J. J., K. SOETAERT, P. M. J. HERMAN, AND C. H. R. HEIP. 1996. Denitrification in marine sediments: A model study. Global Biogeochem. Cycles **10:** 661–673.

MILLERO, F. J., S. SOTOLONGO, AND M. IZAGUIRRE. 1987. The oxidation kinetics of Fe(Ii) in seawater. Geochim. Cosmochim. Acta **51:** 793–801.

NITHART, M., E. ALLIOT, AND C. SALEN-PICARD. 1999. Production, respiration and ammonia excretion of two polychaete species in a north Norfolk saltmarsh. J. Mar. Biol. Assoc. UK **79:** 1029–1037.

SOMMERFIELD, C. K., C. A. NITTROUER, AND C. R. ALEXANDER. 1999. Be-7 as a tracer of flood sedimentation on the northern California continental margin. Cont. Shelf Res. **19:** 335–361.

TEAL, J. M. 1958. Distribution of fiddler crabs in Georgia salt marshes. Ecology **39:** 185–193.

THAMDRUP, B. 2000. Bacterial manganese and iron reduction in aquatic sediments, p. 41–84. *In* B. Schink [ed.], Advances in microbial ecology, v. 16. Kluwer Academic.

VAN CAPPELLEN, P., AND Y. F. WANG. 1996. Cycling of iron and manganese in surface sediments: A general theory for the coupled transport and reaction of carbon, oxygen, nitrogen, sulfur, iron, and manganese. Am. J. Sci. **296:** 197–243.

VERITY, P. G. 2002. A decade of change in the Skidaway River estuary. I. Hydrography and nutrients. Estuaries **25:** 944–960.

ZHANG, J. Z., AND F. J. MILLERO. 1993. The products from the oxidation of H_2S in seawater. Geochim. Cosmochim. Acta **57:** 1705–1718.

Received: 19 September 2003
Amended: 18 May 2004
Accepted: 24 May 2004